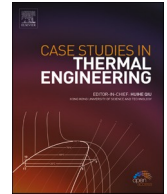




ELSEVIER

Contents lists available at [ScienceDirect](https://www.sciencedirect.com)

Case Studies in Thermal Engineering

journal homepage: www.elsevier.com/locate/csite

Experimental study of optimization of thermoelectric modules' number and layout for waste heat recovery

Xiangrong Ma^a, Shenhua Hu^{b,*}, Wuyuan Hu^c

^a School of Information and Communication Engineering, Nanjing Institute of Technology, Nanjing, 211167, China

^b School of Power and Energy Engineering, Nanjing Institute of Technology, Nanjing, 211167, China

^c Department of Engineering, Durham University, Lower Mount Joy, South Road, Durham, DH1 3LE, UK

ARTICLE INFO

Handling Editor: Huihe Qiu

Keywords:

Thermoelectric generation
Number of modules
Layout of modules
Power distribution

ABSTRACT

A thermoelectric system should be designed in such a way that it harvests as large water heat as possible while using the least modules. To seek an optimal module number, the present study investigates the effect of source temperature, mass flow rate, turbulator, module number and layout on performance of a thermoelectric generator (TEG) system. The experimental results show the optimal module number isn't a fixed value and turbulator has a significant influence on the whole performance of the thermoelectric system. For compact configuration of TEG, using six modules is the best choice without a turbulator, while using eight modules has the best performance with turbulator. The study shows that module layout has a great effect on the thermoelectric system performance. Compared to compact configurations, all separate ones can harvest more power from the hot air except for 32 modules, enhancing by 10–50% whether the turbulator exists or not. In this situation, eight modules are optimal number. The net output power achieves a maximum value of 16.93W and the maximum net efficiency is 3.85% under present experimental parameters. Meanwhile, a new index called power uniformity coefficient is introduced to assess the distribution of output power among TEGs.

Nomenclature

| | |
|-----------|--|
| I_L | Load current (A) |
| MPO | Maximum power output |
| N | Number |
| OCV | Open-circuit voltage |
| P_{out} | Output power (W) |
| P_T | Power loss owing to inserting turbulator (W) |
| P_{net} | Net output power (W) |
| P_{TEG} | Output power of TEG (W) |
| q_W | Volume flow of water (m^3/s) |
| P_W | Pumping power of the cooling water (W) |
| Q | Mass flow rate (kg/h) |

* Corresponding author.

E-mail address: shenhuahu@njit.edu.cn (S. Hu).

<https://doi.org/10.1016/j.csite.2024.104322>

Received 22 January 2024; Received in revised form 21 March 2024; Accepted 30 March 2024

Available online 2 April 2024

2214-157X/© 2024 The Authors. Published by Elsevier Ltd. This is an open access article under the CC BY-NC license (<http://creativecommons.org/licenses/by-nc/4.0/>).

| | |
|--------|------------------------------------|
| Q_1 | Heat transfer rate (W) |
| R | Resistance (Ω) |
| T, t | Temperature ($^{\circ}\text{C}$) |
| VUC | Voltage uniformity coefficient |

Greek symbols

| | |
|----------|---------------------------------|
| α | Seebeck coefficient of TEG, V/K |
| γ | Uniformity coefficient |
| η | Efficiency |

Subscripts

| | |
|--------|---------------------------|
| L | Load |
| $mean$ | Average value |
| P | Power |
| S | Open |
| TEG | Thermoelectric generation |
| U | Voltage (V) |

1. Introduction

Due to numerous advantages such as the absence of moving parts, compactness, silent operation, and high reliability, Thermoelectric Generators/Modules (TEGs/TEMs) applications have become increasingly popular across various industries. A TEG system consists of a heat source, a heat sink, and a TE module positioned between them. This system generates electrical energy through the Seebeck Effect [1]. It occurs when there is a temperature difference across the TEGs.

TEGs can harness electric energy from a wide range of heat sources, including industrial waste heat [2], automotive systems [3], solar energy [4], body heat [5], household stoves [6], geothermal energy [7], and ocean thermal energy [8]. However, it is important to acknowledge that thermoelectric generator systems have certain drawbacks, including low energy efficiency and high cost.

Enhancing energy conversion efficiency and promoting wider adoption of thermoelectric generators have been the focus of numerous studies. These studies aim to address both experimental and theoretical challenges associated with TEG technology. These studies primarily revolve around three key areas: the application of maximum power tracking (MPPT), improving heat-transfer rates at the side of heat source or heat sink of a TE module and optimization of thermoelectric geometry and structure.

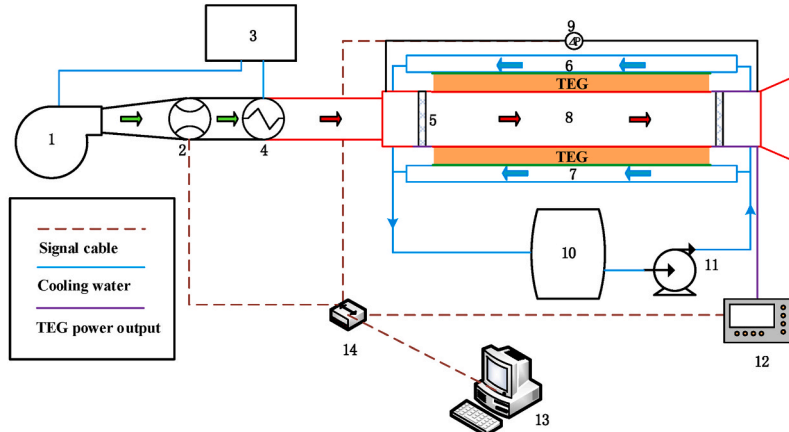
MPPT is a method which is used for optimizing the power output of a TEG by ensuring working condition operate at their maximum power point under varying temperature differences and load resistances. The principle of MPPT involves utilizing an adjustable pulse-width modulation (PWM) to control the switching of a MOSFET in a DC-DC converter. This helps to achieve a match between the inner resistance of the TEG and the load resistance [9,10]. The key aspect of MPPT lies in the design of the control algorithm. Various MPPT methods have been developed and applied in TEG systems. A comprehensive review concerning MPPT methods specific to TEGs was presented by Mamura et al. [11] in 2022. The authors have summarized 62 MPPT methods that have been employed in TEG systems and have recommended several methods that are suitable for TEG applications. Except for MPPT, significant efforts have been devoted to achieving higher temperature differences between hot and cold sides of a TEG. The goal is to enhance the heat energy harvesting capability.

In gas-to-gas TEG heat transfer systems, low convective heat transfer rates can be improved by implementing additional enhancements on the hot gas side. Some methods include adding blocks [12], incorporating stuffing foam metal [13,14], and inserting winglet vortex structures [15,16]. These techniques aim to increase the heat transfer area, disrupt the flow pattern, and enhance convective heat transfer, thereby improving the performance of the TEG system. In liquid-to-liquid TEG systems, varied temperature conditions [17] and flow rates [11] are commonly used in experimental setups. These factors have been extensively studied to optimize the performance of the TEG system. The high output power obtained from these systems has contributed to their potential for commercialization.

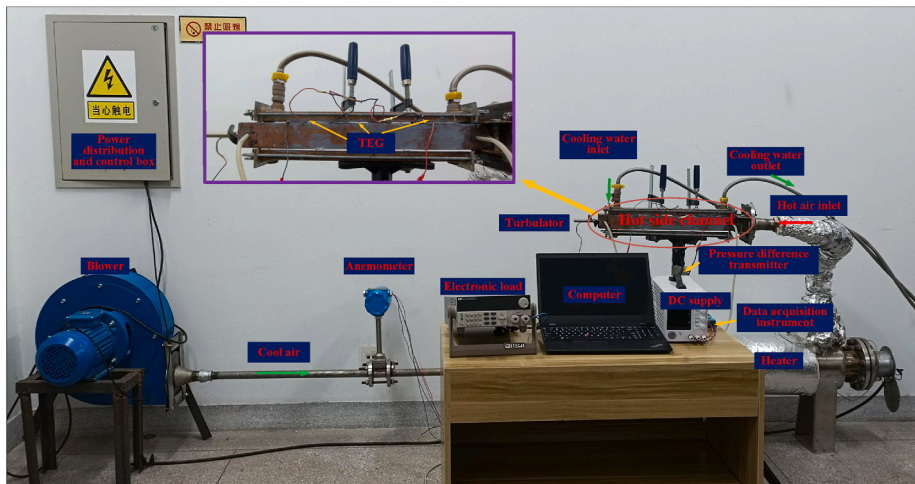
Indeed, there have been significant theoretical contributions focused on optimizing the geometry and structure of thermoelectric modules [18]. In the context of hybrid PV-TE (photovoltaic-thermoelectric) systems, researchers have investigated various aspects to improve their performance and efficiency. Cui et al. [19] conducted studies on hybrid PV-TE systems and found that the optimum height of the thermoelectric module decreased with the height ratio of the upper to lower thermoelectric leg. They also observed that the length of the thermoelectric leg had little influence on the optimized height of the module. Furthermore, they discovered that the optimized height of the thermoelectric module decreased with increased concentrated solar radiance. Shittu et al. [20] utilized the Finite Element Method to investigate the optimum geometry for maximum efficiency of a hybrid PV-TE uni-couple. Their results demonstrated that a symmetrical thermoelectric leg geometry yielded better performance for the hybrid PV-TE system. Lakeh et al. [21] mathematically modelled and simulated a novel integrated TE-PV cell. They determined optimum ranges for factors such as the number of thermoelectric couples and the cross-sectional area, aiming to maximize the system's performance. Xuan et al. [22] constructed a thermal-electric coupled model of thermoelectric generators to investigate the thermoelectric performance under nonuniform solar radiation. These findings highlighted the importance of considering the concentration ratio and nonuniformity in the

design and optimization of solar thermoelectric generators. Considering the Thomson effect, Lamba et al. [23] developed a thermodynamic model for an extensible thermoelectric cooler. They optimized the cooling capacity and energy efficiency using a genetic algorithm. He et al. [24] investigated the effect of gas parameters on the optimal thermoelectric performance to maximize the total output power in an exhaust system. They found that optimizing the module area played a crucial role in achieving the maximum thermoelectric performance. Additionally, they discovered that the optimal module areas were significantly influenced by the flow rate of the exhaust gas, but not by the gas temperature. These studies contribute to the understanding and optimization of various factors pertaining to the geometry, structure, and performance of hybrid PV-TE systems, offering valuable insights for enhancing their efficiency and output power.

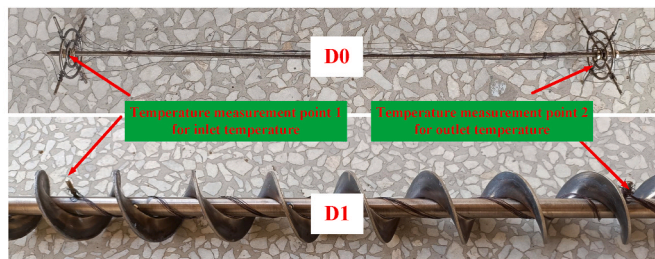
The output voltage and current are typically small for a thermoelectric module. To increase the output power, it is common to



1. blower; 2. anemometer; 3. power distribution and control box; 4. heater; 5. strainer; 6, 7. water cooling; 8. hot side channel; 9. pressure difference transmitter; 10. water-cooling chiller; 11. pump; 12. electronic load; 13. computer; 14. data acquisition instrument.
(a) Schematic diagram of thermoelectric system



(b) System setup



(c) Temperature measurement point distribution for inlet and outlet air

Fig. 1. Experimental system of thermoelectric generator.

connect multiple TE modules in series or parallel configurations. The optimization of multi-TEG systems has been a central focus in numerous research works. Jin et al. [25] conducted experimental investigations to optimize the geometry of thermoelectric modules. They used three modules with different geometries and proposed improvements based on their experimental results. Negash et al. [26] performed experiments to investigate the effect of the electrical array configuration of TEGs on thermoelectric power generation. They formed eight different array configurations using 10 TE modules connected in series, parallel, and combination connections. They concluded that an array configuration with a minimized number of junctions and a balanced number of modules was recommended for maximizing the TEG power output. Jang et al. [27] studied the optimization of TEG module spacing and spreader thickness in a waste heat recovery system. They developed numerical models and validated them with experimental data. The predicted numerical data were in good agreement with the experimental results. Favarel et al. [28] developed a computer model to study the influence of TEG position on optimizing electrical power. Their simulation showed that each thermoelectric fabrication had an optimal occupancy rate for maximizing power output. Alvaro et al. [29] conducted a computational study to optimize the configuration of a TEG for waste heat recovery from hot fumes. They validated their computational model by building an optimized TEG configuration. The potential power harvested using the validated computational model was estimated to be up to 30.8 MWh throughout the year. Rattner et al. [30] developed a model to predict the behavior of TEG arrays with varying module counts at low and high fluid thermal capacity rates. The model could identify the optimal number of TEGs for designing a waste heat recovery system. Miguel et al. [31] combined two computational models to optimize TEGs at a stone wool manufacturing plant. The results indicated that the occupancy ratio of the TEGs had a significant effect on the output power. A low occupancy ratio resulted in small power generation, while a high occupancy ratio could lead to reaching the outlet temperature limit. Zhao et al. [32] proposed a model for an exhaust thermoelectric generator (TEG) and made an energy and exergy analyses to assess its performance. According to the results, the primary exergy losses were attributed to convective heat transfer and PN junction thermal conductivity. These findings help in understanding the thermodynamic characteristics of the TEG system and provides a foundation for developing high-efficiency exhaust power generators. Patricia et al. [33] proposed the use of TEGs for geothermal energy using phase-change heat exchangers. They conducted laboratory experiments by varying the number of TE modules and the temperature of the heat source. The results showed that using more modules decreased the efficiency per module, but the total power increased for the number of modules tested. He et al. [34] explored the influence of circuit layout on TEG performance in an exhaust system. They focused on addressing TEG power output performance and optimal structure scales under different circuit layouts. They recommended applying a multi-stage series current mode for large-scale TEG systems due to the significant enhancement in power. Ge et al. [35] experimentally investigated the effects of hot air temperature, flow rate, and the number of modules on thermoelectric performance. The results showed that power harvested increased with the number of TEG modules under high-flow conditions. These studies highlight the importance of optimizing the configuration, geometry, and array layout of TEG systems to maximize their power output and overall performance. By understanding these factors, researchers can improve efficiency of thermoelectric energy conversion.

There is indeed a wealth of literature focusing on the recovery of waste heat from automotive exhausts, which typically have high temperatures ($>350\text{ }^{\circ}\text{C}$) and large flow rates ($>80\text{ kg/h}$) [36]. However, there is relatively less attention given to the utilization of waste heat from domestic sources where temperatures may not be high and flow rates may not be large. Furthermore, in most studies, the number and position of thermoelectric elements are fixed, without taking into account the influence of turbulators on the optimal number of thermoelectric elements in a system.

In our study, an experimental setup is designed and constructed to investigate the power distribution characteristics, and the impact of various factors on the performance of the thermoelectric system. The experiments were conducted under different experimental conditions, including a range of hot air temperatures ($150\text{--}350\text{ }^{\circ}\text{C}$), mass flow rates ($12\text{--}48\text{ kg/h}$), module numbers (3-32) and different module arrangements (6 types) with or without a turbulator.

2. Thermoelectric generation experimental system

2.1. Experimental system

The experimental system consists of several components: a hot air supply source, a test section, thermoelectric generators, a cooling water tank, and data acquisition equipment. The schematic diagram and system setup are illustrated in Fig. 1(a) and (b) (The upper left part is a partially enlarged photo of the test section), respectively. The hot air supply source is responsible for providing heated air to the test section. It utilizes a high-precision heater with a power range of $0\text{--}6\text{ kW}$ and an accuracy of $\pm 1\text{ }^{\circ}\text{C}$. The heater is controlled by a thyristor, which allows for precise adjustment of the hot air temperature. By adjusting the thyristor, a specific temperature value can be set and maintained automatically. The air flow in the system is regulated by a blower, which is controlled by an inverter. The inverter enables the adjustment of the blower's rotational speed, thereby controlling the air flow rate through the system. This feature allows for flexibility in setting the desired air flow rate during the experiments. In the test section, the heated air enters the hot side channel, where it comes into contact with the TEGs. The TEGs are responsible for converting the temperature difference between the hot air and the ambient environment into electrical power. As the hot air passes through the TEGs, it releases heat, which is converted into electrical energy. After passing through the TEGs, the air flows out into the ambient environment.

In the TEG test section, the main components include a copper square duct, four rectangular copper ducts, TE modules, heat exchangers, insulation cotton, thermocouples, a thermal type gas flowmeter, a turbine flowmeter, and a pressure differential transmitter. The test section consists of a copper square duct with specific dimensions. It has a length of 550 mm , a cross-section of $50\text{ mm} \times 50\text{ mm}$, and a wall thickness of 2 mm . This duct serves as the main channel for the hot air flow. There are four rectangular copper ducts used as heat sinks. Each duct has a length of 400 mm and a cross-section of $20\text{ mm} \times 40\text{ mm}$. These ducts help dissipate the heat absorbed by the TEGs. Thermoelectric modules, specifically the TG 12-6 model from Marlow Industries Inc., are used in the experiment. These

modules are sandwiched between the hot-side and cold-side heat exchangers symmetrically on each side of the copper square duct. The specifications of the TG 12-6 module can be found in Table 1. Heat exchangers are used on both the hot side and cold side of the TE modules. These exchangers facilitate heat transfer between the hot air and the TEGs on the hot side and between the TEGs and the cooling water.

on the cold side. To minimize heat loss, 5 cm thick insulation cotton is wrapped around the electric heating pipes and the inlet pipe. This insulation helps maintain the desired temperature gradient and prevents unnecessary heat dissipation. Four thermocouples are used to measure the inlet and outlet air temperatures (Fig. 1(c)). These thermocouples provide temperature data that is essential for calculating the conversion efficiency of the TEG system. A thermal type gas flowmeter (MIK-MF) with a range of 0–70 kg/h and an accuracy of 1% is employed to monitor the rate of the air flow through the system. It measures the mass flow rate of the hot air. A turbine flowmeter (LWGY) with a range of 0.2–1.2 m³/h and an accuracy of 0.5% is used to monitor the flow rate of the cold-side cooling water. It measures the volumetric flow rate of the cooling water. A pressure differential transmitter (HALO-FY-WG) with a range of 0–400 Pa and an accuracy of 0.2% is deployed to measure the air pressure difference in the test section. This transmitter helps monitor and analyze the air pressure distribution within the system. These components, along with the data collected from the thermocouples and flowmeters, enable the measurement and analysis of important parameters necessary to evaluate the performance of the TEG system, including temperature differentials, air flow rate, and cooling water flow rate.

2.2. The TEG electrical layout type

To comprehensively assess the effect of the number of TEGs on the thermoelectric performance. A wide range of TEG numbers ranging from 32 to 3 have been chosen for experimental investigation. The experimental setup allows for various configurations of TEG layouts based on the number of modules. The TEG modules can be assembled on four, two, or one side of the copper square duct, while the remaining region is carefully covered with insulating material to minimize heat loss. Considering the performance differences among the TEGs and the experimental conditions, six specific TEG numbers are determined to study this issue. The layouts of the TEGs are illustrated in Fig. 2. Each configuration is designated by a number followed by "N," representing the TEG number. The "CO" configuration refers to an intimate arrangement among the TE modules, distinguishing it from non-intimate configurations.

2.3. Flow turbulator inserts

To investigate the impact of a turbulator on the heat transfer characteristics of the air within the system. Specifically, a Twisted Tape turbulator is selected for this purpose. The Twisted Tape turbulator consists of a strip made of stainless steel with a pitch of 50 mm, a strip width of 47 mm, and a thickness of 3 mm, as shown in Fig. 3. This turbulator can be easily inserted into the duct to enhance heat transfer. The use of a turbulator in the duct is known to increase heat transfer rates by promoting turbulence and enhancing fluid mixing. This improvement in heat transfer comes at the expense of additional pressure drops within the system. The increased pressure drops result in additional energy losses, which can impact the overall power generation of the thermoelectric system.

2.4. Experimental procedure and data reduction

Our experiment investigates the output power of the TEGs in relation to the load resistance or load current. To conduct this study, certain experimental conditions have been selected, including variations in the inlet air temperature and mass flow rate. The specific experimental conditions and their corresponding numbers are listed in Table 2 and Table 3, respectively. The inlet air temperature ranges from 150 °C to 350 °C and the mass flow rate varies from 12 kg/h (0.0033 kg/s) to 48 kg/h (0.0133 kg/s). These variations in temperature and mass flow rate allow for a comprehensive analysis of their impact on the TEGs' output power. This system enables the recording and monitoring of the current and voltage values as the load resistance is adjusted. Additionally, we also measure the mass flow rate of the air and monitor the pressure drop in the duct.

In the experiment, we follow these procedures: (1) Set desired temperature and mass flow rate of the inlet air before starting the experiment. (2) Once the desired temperature and mass flow rate are set, turn on the heater to start heating process within the system. (3) When the inlet air temperature is close to the set value turn on the cooling water. This helps maintain the desired temperature and prevents overheating. (4) After the inlet air temperature has reached a stable state, the data acquisition system starts recording data at regular intervals of 5 s. This includes measurements of various parameters such as current, voltage, mass flow rate, and pressure drop. Throughout the experiment, the rate of cooling water from the chiller is maintained at 6.7 L/min, and its temperature is kept at 290 K. By following these procedures, we ensure that the system reaches a steady state before data collection begins.

The pumping power is defined as:

Table 1
The specification of TG 12-6.

| Parameter | Value |
|----------------------------|---------------|
| Model | TG 12-6 |
| Dimensions (cm) | 4.5 × 4 × 0.4 |
| Hot side temperature (°C) | 230 |
| Cold side temperature (°C) | 50 |
| Open circuit voltage (V) | 9.51 |
| Max Power (W) | 6.16 |
| Efficiency, η (%) | 5.03 |

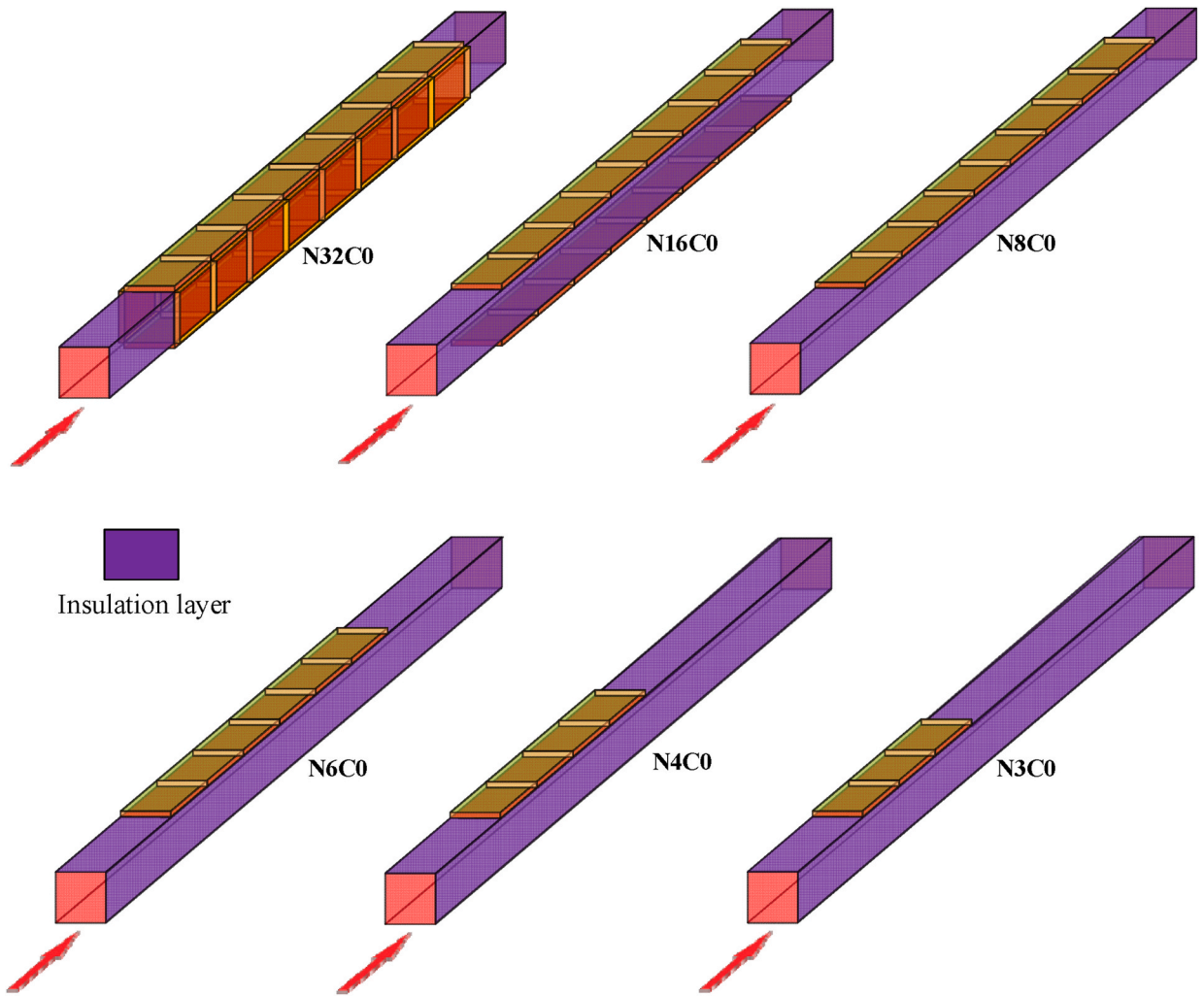


Fig. 2. TEG allocation Arrows indicate a ring of TEG.

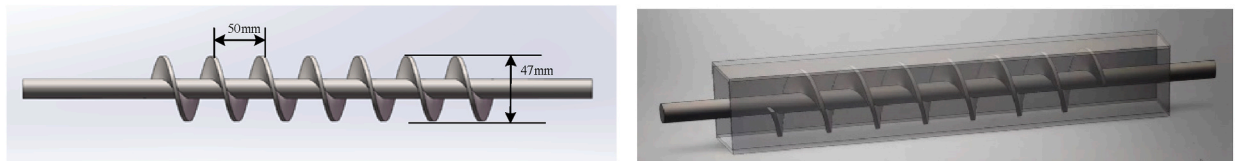


Fig. 3. Removable flow twisted tape turbulator (D1).

Table 2
Main experimental parameters.

| Type | Unit | Value |
|----------------------------|--------------------|-----------------------|
| Air inlet temperature T | $^{\circ}\text{C}$ | 150, 250, 350 |
| Air flow Q | kg/h | 12, 24, 36, 48 |
| Number of module N | – | 3, 4, 6, 8, 16, 32 |
| With turbulator or not D | – | 0 (without), 1 (with) |

Table 3
Corresponding order number of working conditions.

| Order number | Working conditions | Order number | Working conditions | Order number | Working conditions |
|--------------|--------------------|--------------|--------------------|--------------|--------------------|
| 1 | T150Q12D0 | 9 | T250Q12D0 | 17 | T350Q12D0 |
| 2 | T150Q24D0 | 10 | T250Q24D0 | 18 | T350Q24D0 |
| 3 | T150Q36D0 | 11 | T250Q36D0 | 19 | T350Q36D0 |
| 4 | T150Q48D0 | 12 | T250Q48D0 | 20 | T350Q48D0 |
| 5 | T150Q12D1 | 13 | T250Q12D1 | 21 | T350Q12D1 |
| 6 | T150Q24D1 | 14 | T250Q24D1 | 22 | T350Q24D1 |
| 7 | T150Q36D1 | 15 | T250Q36D1 | 23 | T350Q36D1 |
| 8 | T150Q48D1 | 16 | T250Q48D1 | 24 | T350Q48D1 |

$$P_w = q_w \Delta p \tag{1}$$

where q_w is the volume flow rate of cooling water and Δp is the pressure drop in the test section.

Increasing the rate of cooling water results in a higher power output from the waste heat. However, it is important to note that higher flow rates also require more pumping power to maintain the desired flow rate. Therefore, there exists an optimum flow rate that maximizes the output power while considering the pumping power consumption. Based on previous experiments, the optimum flow rate for the system is 6.7 L/min. The corresponding pumping power is 0.21W from Eq.(1).

The efficiency of the TEG is:

$$\eta = \frac{P_{TEG}}{Q} \tag{2}$$

where η is the efficiency of the TEG, Q is the heat transfer rate through the contact interface, P_{TEG} is the total output power of the TEG.

The net power output is defined as:

$$P_{net} = P_{TEG} - P_w - P_T \tag{3}$$

Where P_T is power loss owing to inserting the turbulator in the test section.

The net efficiency of the total TEG is:

$$\eta_{net} = \frac{P_{net}}{Q} \tag{4}$$

For examining the distribution of the TEG performance, an index, the voltage uniformity coefficient (VUC) of the TEGs γ_U , was proposed to evaluate the uniformity of the generator voltage distribution [35], the formula is as follows:

$$\gamma_U = 1 - \frac{1}{n} \sum_{i=1}^n \frac{\sqrt{(U_{n,i} - U_{mean})^2}}{U_{mean}} \tag{5}$$

Where U_n is the circuit terminal voltage of all modules, U_{mean} is the average voltage of modules.

An uncertainty analysis is done according to Kline and McIntock [37], and the results show that uncertainties for the power output

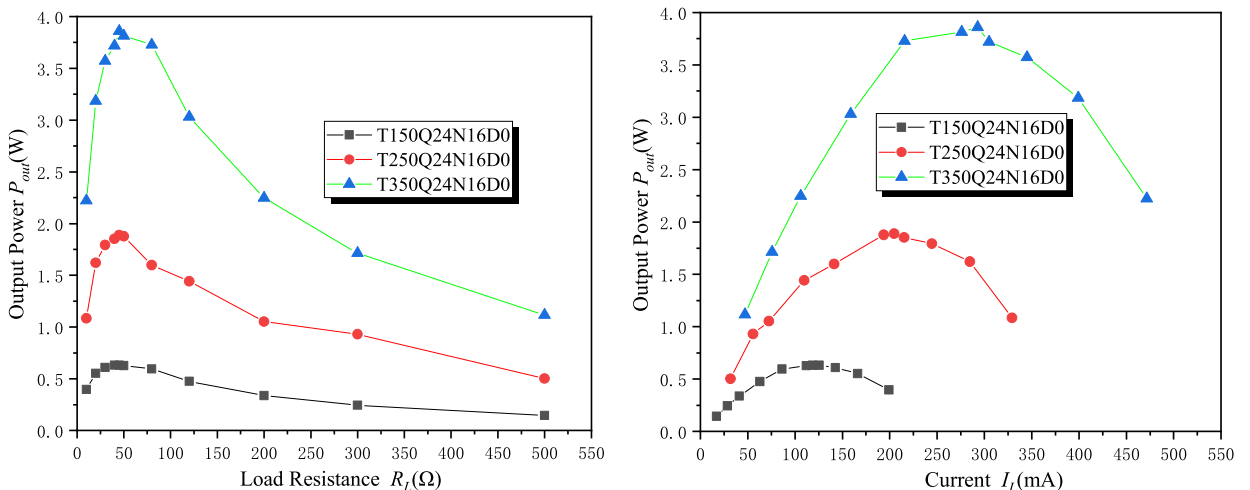


Fig. 4. Electric power output against load resistance/current for different air temperature.

of 1% and for the net power output of 4.02%.

3. Result and discussion

The arrangement of TEG can be classified into intimate and non-intimate configuration in our study. So, we discuss experimental results from two parts in the following. The effect of inlet air temperature, mass flow rate and insert on output power are briefly introduced before discussion.

3.1. The effect of inlet air temperature, mass flow rate and insert on output power

Based on the comparison of experiments using different inlet air temperatures, it is evident that the temperature has a significant influence on the characteristics of the TEG. The findings are presented in Fig. 4, which depicts the load resistance (left) and current (right) as functions of the output power for inlet air temperatures of 150 °C, 250 °C, and 350 °C, respectively. The results clearly demonstrate that higher temperatures lead to a substantial improvement of the output power of the TEG. Regardless of the particular temperature, the curves consistently exhibit the same trend. In the absence of a turbulator, the peak power values are 1.71 W, 4.87 W, and 9.63 W for inlet air temperatures of 150 °C, 250 °C, and 350 °C, respectively. This indicates a relative variation rate of 184% and 97% between the lowest and highest temperatures.

Fig. 5 presents the effect of mass flow rate on the output power of the TEG, and the experimental results demonstrate that the mass flow rate has a significant impact on TEG performance. The findings likely indicate that higher mass flow rates lead to improved heat transfer and larger temperature differences, resulting in higher output power.

In the experiment, the insertion of a turbulator in the duct creates turbulence in the core flow, leading to disturbances near the duct wall. This turbulence generates vortex motion, resulting in enhanced convective heat transfer near the heated wall. The experimental results, as shown in Fig. 6, support the fact that the turbulator improves convective heat transfer. To further analyze the impact of the turbulator, the Reynolds number (Re) is calculated and presented in Fig. 6. The results indicate that the insertion of the turbulator increases the Re number by nearly three times under the same operating conditions.

3.2. The power uniformity coefficient

For examining the distribution of the TEG performance in series, the voltage uniformity coefficient (VUC) is calculated using Eq. (5) for two cases: open circuit and maximum power output, as shown in Fig. 7. The figure illustrates the VUC as a function of the module number under six different conditions. The left picture shows the VUC for the open circuit case and the right figure represents the VUC for the maximum power output (MPO) case. The VUC quantifies the uniformity of the voltage distribution among the modules of the thermoelectric system. According to the figure, both γ_{OCV} (VUC for the open circuit) and γ_{MPO} (VUC for the maximum power output) decrease as the module number increases. This suggests that larger systems with more modules tend to exhibit less uniform voltage distribution. For a given module number, the VUC increases with increasing air mass rate and the addition of a turbulator. This means that higher air mass rates and the presence of a turbulator contribute to a more even voltage distribution among the modules. Specifically, the VUC has the highest value when the circuit is open, indicating the most uniform voltage distribution. As the load current increases, the VUC decreases, implying a decrease in voltage uniformity. A VUC value equal to one indicates complete uniformity, where every module has the same voltage [35].

Regarding the power uniformity coefficient (γ_p), it is introduced as a new index to assess the difference in output power distribution within a TEG system. The power uniformity coefficient quantifies the variation in power generation among the individual modules within the system.

The power uniformity coefficient, γ_p , can be calculated using the following equation:

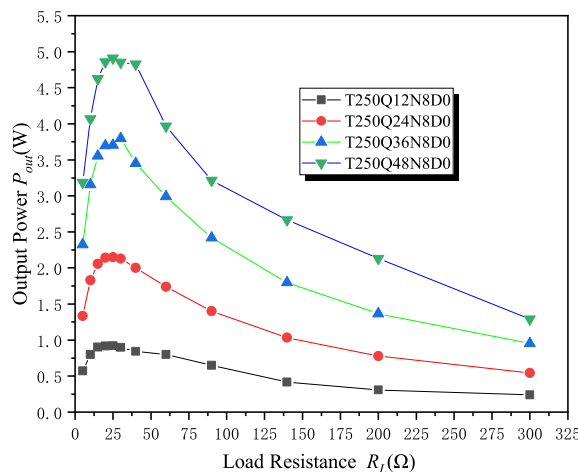


Fig. 5. Electric power output against load resistance for different flow rate.

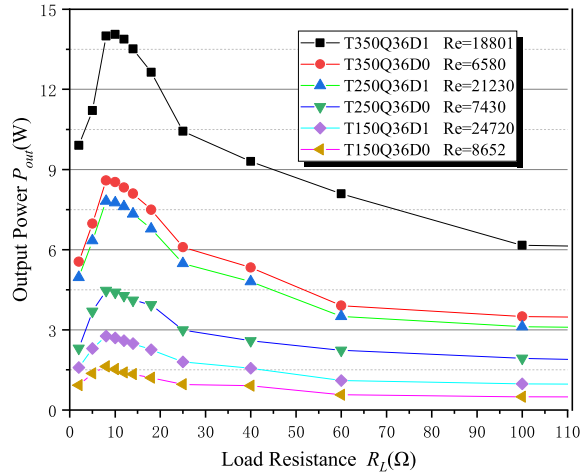


Fig. 6. Electric power output against load resistance for with or without turbulator.

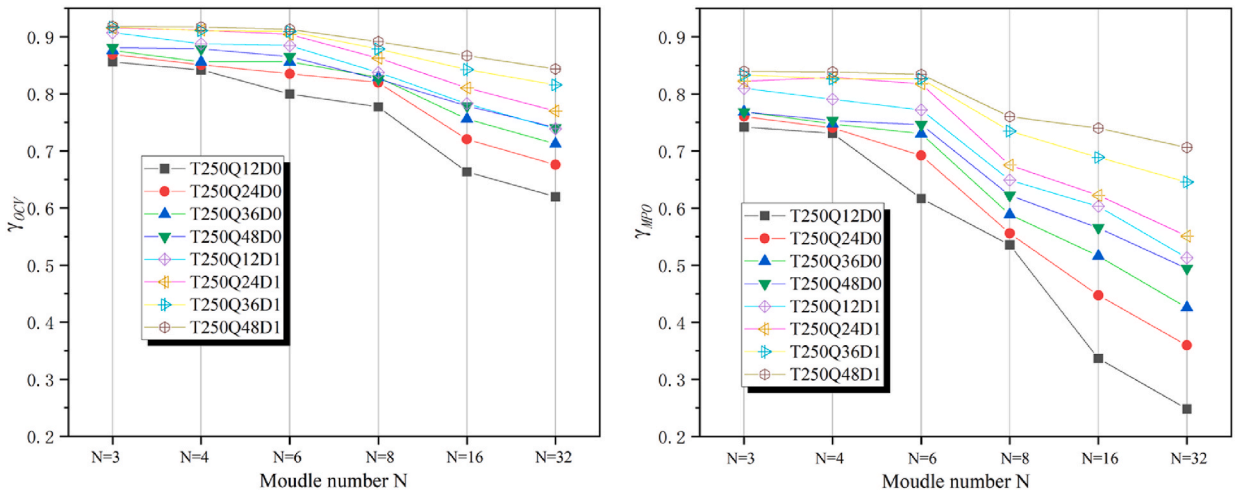


Fig. 7. Voltage uniformity coefficient for open circuit (left) and maximum power point (right).

$$\gamma_p = 1 - \frac{1}{n} \sum_{i=1}^n \frac{\sqrt{(P_{TEM,i} - P_{mean})^2}}{P_{mean}} \tag{6}$$

In the equation, all the power terms represent the maximum output power. While the voltage uniformity coefficient (γ_U) and the power uniformity coefficient (γ_p) have the same value in a series circuit, γ_p is considered to be more comprehensible and intuitive for the TEG system. It provides a measure of the disparity in power output among the modules.

To illustrate this, let's consider an example with $N = 32$ modules. The lowest mass rate without the turbulator will have the minimum power uniformity coefficient, indicating the maximum discrepancy in power output among the modules. As the mass flow rate increases, the deviation in output power among the TEGs gradually decreases. When the turbulator is added to the channel, it intensifies the turbulence, resulting in a more uniform distribution of power among the modules.

In summary, γ_p has close association with the module number and experimental condition, when the number of thermoelectric elements is reduced, and the temperature and flow rate are increased while maintaining strong turbulence, the deviation between the power output of each thermoelectric element and the average power output will be minimized.

3.3. Intimate arrangement of thermoelectric generators

3.3.1. The effect of number module on output power without insert

In Fig. 8, the maximum output power of the TEG system is depicted under different experimental conditions, taking into account varying numbers of modules. The aim of determining the number of modules is to optimize the output power and achieve the highest possible economic efficiency.

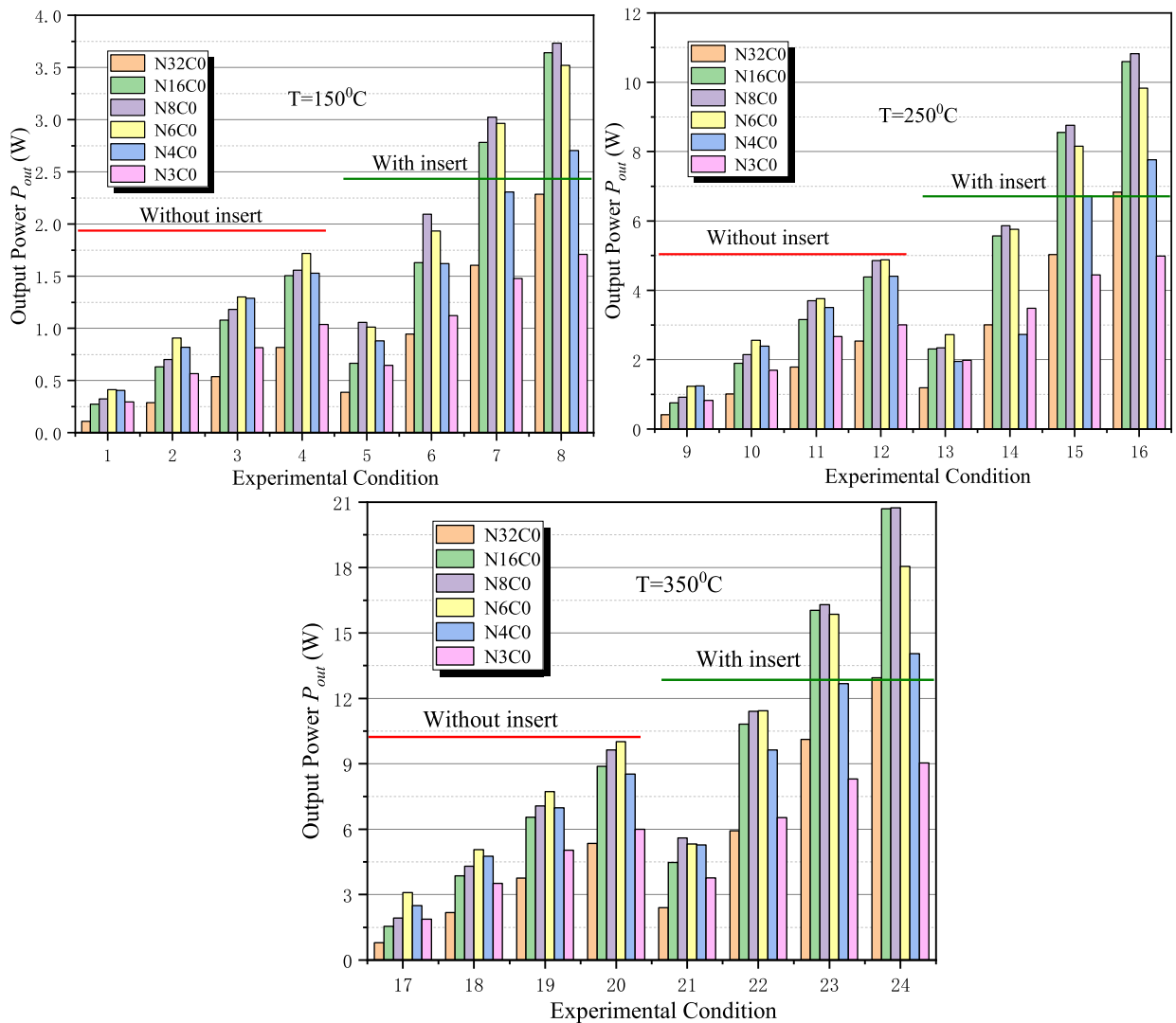


Fig. 8. MPO of different number modules under different experimental conditions.

By examining Fig. 8, it is evident that the output power increases as the inlet temperature and the mass flow rate of the air increase. This indicates that higher inlet temperatures and higher mass flow rates result in greater power generation within the TEG system. For instance, considering an inlet air temperature of 350 °C, when the number of modules is 32, 16, 8, 6, and 4, and the air flow rate ranging from 12 kg/h to 48 kg/h, the output power increases by factors of 6.1, 5.8, 5.3, 4, 3.5, and 3.6, respectively. This demonstrates that increasing mass flow rate leads to a significant increase in output power. However, it's worth noting that a larger number of modules does not necessarily translate to greater electric energy harvested from waste heat. In the case of 32 and 16 modules, especially 32 modules, the experimental parameters indicate that these scenarios are not acceptable. Interestingly, as the number of TEG modules decreases, the output power gradually increases until reaching a maximum at six modules. After that point, the power begins to decrease. This suggests that there is an optimal number of modules that maximizes the output power, and exceeding or falling short of this optimal number leads to a decrease in power generation. From above research, determining the appropriate number of modules within the TEG system is crucial for achieving the highest output power while considering economic efficiency.

3.3.2. The effect of number module on output power with insert and optimal TEG number

Adding a turbulator in the channel is indeed an effective method to enhance heat transfer, resulting in increased power generation from hot air. Comparing the output power with and without a turbulator from Fig. 8, it is evident that the presence of a turbulator leads to higher output power. To illustrate this, let's consider an example where the temperature (T) is 350 °C, and the number of modules (N) is 8. When the air flow rate ranges from 12 kg/h to 48 kg/h, the output power increases by factors of 2.76, 2.64, 2.31, and 2.15, respectively, compared to the case without a turbulator.

Additionally, the optimal module number changes from six to eight when a turbulator is added. However, it is important to note

that the presence of a turbulator also introduces additional pressure drop from the inlet to the outlet of the duct. This results in a decrease in effective electronic power, which can be calculated using Eq. (3). The decrease in effective electronic power is attributed to the presence of the turbulator and the associated pumping power required. To improve the cooling effect, a larger cooling water flow rate is necessary. However, beyond a certain point, further increases in the cooling water flow rate have minimal contributions to increasing the output power. Moreover, a higher cooling water flow rate leads to higher energy consumption. As mentioned in section 2.4, a cooling water flow rate of 6.7 L/min is confirmed as the optimum value. At this flow rate, the corresponding pressure drop measured results in a pumping power of 0.21 W.

When adding a turbulator in the channel, the situation is different. With the addition of a turbulator, it is found that eight modules are the optimal choice in terms of maximizing the power harvested from hot air compared to other scenarios. The phenomenon is attributed to the low heat transfer and heat capacity of the air, which ultimately affects the system's performance.

When a higher number of modules are connected in series, the internal resistance increases, which may lead to that the load current is less than the short-circuit current of the TEGs. Therefore, the power generated by the TEGs cannot meet the power consumption of the internal resistance, resulting in some TEGs acting as loads and causing power loss. Another factor is the rapid drop in wall temperature along the direction of air flow, causing the TEGs in the downstream to compete for heat with the TEGs in the upstream. This competition decreases the temperature difference across the TEGs in the upstream, impacting their power generation capability [38]. Considering these factors, it is evident that the optimal number of modules and the presence of a turbulator can significantly affect the power generation and efficiency of the TEG system.

3.3.3. Performance index for some experimental conditions

Turbulators have a significant impact on various aspects of the thermoelectric system, including the temperature difference (TD) in the channel, output power, efficiency, and other parameters. Table 4 provides detailed information on specific experiments,

Table 4
Summary of performance index.

Table.4 Summary of performance index

| Experimental condition | N | TD ($^{\circ}\text{C}$) | P_{TEG} (W) | Δp (Pa) | P_W (W) | P_A (W) | P_{net} (W) | P_{per} (W) | $P_{per,net}$ (W) | η | η_{net} |
|------------------------|-----|---------------------------|---------------|-----------------|-----------|-----------|---------------|---------------|-------------------|--------|--------------|
| T150Q48D0 | 32 | 11.34 | 0.82 | 0 | 0.21 | 0 | 0.61 | 0.03 | 0.02 | 0.53 | 0.40 |
| | 16 | 10.41 | 1.50 | 0 | 0.21 | 0 | 1.29 | 0.09 | 0.08 | 1.05 | 0.91 |
| | 8 | 8.43 | 1.56 | 0 | 0.21 | 0 | 1.35 | 0.19 | 0.17 | 1.37 | 1.18 |
| | 6 | 7.76 | 1.72 | 0 | 0.21 | 0 | 1.51 | 0.29 | 0.25 | 1.65 | 1.44 |
| | 4 | 7.65 | 1.53 | 0 | 0.21 | 0 | 1.32 | 0.38 | 0.33 | 1.49 | 1.28 |
| | 3 | 5.16 | 1.04 | 0 | 0.21 | 0 | 0.83 | 0.35 | 0.28 | 1.49 | 1.19 |
| T150Q48D1 | 32 | 34.15 | 2.28 | 252.3 | 0.21 | 3.70 | -1.62 | 0.07 | -0.05 | 0.49 | -0.35 |
| | 16 | 32.24 | 3.64 | 248.9 | 0.21 | 3.61 | -0.18 | 0.23 | -0.01 | 0.83 | -0.04 |
| | 8 | 30.60 | 3.73 | 249.4 | 0.21 | 3.66 | -0.14 | 0.47 | -0.02 | 0.89 | -0.03 |
| | 6 | 20.79 | 3.52 | 190.0 | 0.21 | 2.86 | 0.45 | 0.59 | 0.07 | 1.25 | 0.16 |
| | 4 | 17.03 | 2.70 | 122.6 | 0.21 | 1.84 | 0.65 | 0.68 | 0.16 | 1.18 | 0.28 |
| | 3 | 16.46 | 1.71 | 91.3 | 0.21 | 1.36 | 0.14 | 0.57 | 0.05 | 0.78 | 0.06 |
| T250Q24D0 | 32 | 42.08 | 1.01 | 0 | 0.21 | 0 | 0.80 | 0.03 | 0.03 | 0.35 | 0.28 |
| | 16 | 32.09 | 1.90 | 0 | 0.21 | 0 | 1.69 | 0.12 | 0.11 | 0.85 | 0.75 |
| | 8 | 26.01 | 2.14 | 0 | 0.21 | 0 | 1.93 | 0.27 | 0.24 | 1.19 | 1.07 |
| | 6 | 20.62 | 2.56 | 0 | 0.21 | 0 | 2.35 | 0.43 | 0.39 | 1.99 | 1.83 |
| | 4 | 20.08 | 2.39 | 0 | 0.21 | 0 | 2.18 | 0.60 | 0.54 | 1.73 | 1.58 |
| | 3 | 12.75 | 1.70 | 0 | 0.21 | 0 | 1.49 | 0.57 | 0.50 | 1.93 | 1.69 |
| T250Q24D1 | 32 | 82.37 | 3.00 | 42.73 | 0.21 | 0.73 | 2.06 | 0.09 | 0.07 | 0.53 | 0.37 |
| | 16 | 76.29 | 5.57 | 42.31 | 0.21 | 0.72 | 4.64 | 0.35 | 0.29 | 1.04 | 0.87 |
| | 8 | 73.77 | 5.96 | 40.46 | 0.21 | 0.70 | 5.06 | 0.73 | 0.63 | 1.17 | 1.0 |
| | 6 | 61.35 | 5.76 | 30.06 | 0.21 | 0.53 | 5.02 | 0.96 | 0.84 | 1.38 | 1.20 |
| | 4 | 54.19 | 2.73 | 20.39 | 0.21 | 0.36 | 1.38 | 0.49 | 0.34 | 0.52 | 0.37 |
| | 3 | 50.60 | 3.48 | 15.23 | 0.21 | 0.27 | 3.00 | 1.16 | 1.00 | 0.99 | 0.86 |
| T350Q12D0 | 32 | 57.90 | 0.80 | 0 | 0.21 | 0 | 0.59 | 0.02 | 0.02 | 0.39 | 0.29 |
| | 16 | 56.31 | 1.55 | 0 | 0.21 | 0 | 1.34 | 0.10 | 0.08 | 0.77 | 0.66 |
| | 8 | 30.95 | 1.93 | 0 | 0.21 | 0 | 1.72 | 0.24 | 0.21 | 1.84 | 1.64 |
| | 6 | 31.60 | 3.09 | 0 | 0.21 | 0 | 2.88 | 0.51 | 0.48 | 2.61 | 2.43 |
| | 4 | 31.99 | 2.49 | 0 | 0.21 | 0 | 2.28 | 0.62 | 0.57 | 2.12 | 1.94 |
| | 3 | 22.45 | 1.87 | 0 | 0.21 | 0 | 1.66 | 0.62 | 0.55 | 2.34 | 2.08 |
| T350Q12D1 | 32 | 145.43 | 2.40 | 10.92 | 0.21 | 0.19 | 2.00 | 0.08 | 0.06 | 0.47 | 0.39 |
| | 16 | 131.87 | 4.48 | 10.57 | 0.21 | 0.19 | 4.08 | 0.28 | 0.25 | 0.94 | 0.86 |
| | 8 | 98.06 | 5.59 | 10.20 | 0.21 | 0.19 | 5.18 | 0.67 | 0.65 | 1.55 | 1.51 |
| | 6 | 81.81 | 5.32 | 7.61 | 0.21 | 0.15 | 4.97 | 0.93 | 0.83 | 1.98 | 1.77 |
| | 4 | 83.03 | 5.27 | 5.06 | 0.21 | 0.10 | 4.97 | 1.32 | 1.24 | 1.83 | 1.72 |
| | 3 | 82.44 | 3.76 | 3.76 | 0.21 | 0.07 | 3.48 | 1.25 | 1.16 | 1.21 | 1.12 |

highlighting the effects of the turbulator. The information provided in Table 4 allows for a detailed analysis of the effects of the turbulator on various parameters and power losses within the thermoelectric system. From Tables 4, it is evident that regardless of the module number, the presence of a turbulator results in higher electrical power compared to the case without a turbulator. Additionally, the TD in the channel generally increases with the module number. This indicates that, all else being equal, the presence of a turbulator leads to a greater temperature difference across the channel.

There are two types of power losses to be considered: pumping power (P_W) and pressure drop in the channel (P_T). The pumping power, determined by the optimum cooling water flow rate, remains constant in all experiments. However, the pressure drop (P_T) is closely associated with the air flow rate and module number. In cases where the inlet temperature is low and the mass flow rate is high, the power loss cannot be significant enough to surpass the output power of the TEGs. As a result, the total power system becomes a load rather than a source of power generation as mentioned before. These scenarios are highlighted in Table 4 using red boxes to indicate the cases where power losses outweigh the output power. It is important to note that when working with different numbers of modules, high efficiency does not always correspond to a higher power recovery. The primary objective is to maximize output power while using as few modules as possible. In this context, the net output power becomes more meaningful in practical terms than the power generated by the TEGs alone. By considering the net output power, one can evaluate the system's efficiency in terms of power recovery, accounting for factors such as power losses due to the presence of a turbulator, pressure drop, and other considerations.

3.4. Non-intimate arrangement of thermoelectric generators

3.4.1. Non-intimate arrangement methods

In the subsequent section, the study shifts focus to the layout of the TEGs and its effect on output power. By exploring different TEG layouts, the study aims to investigate how the arrangement of TEGs impacts the output power of the system. Fig. 9 illustrates a new

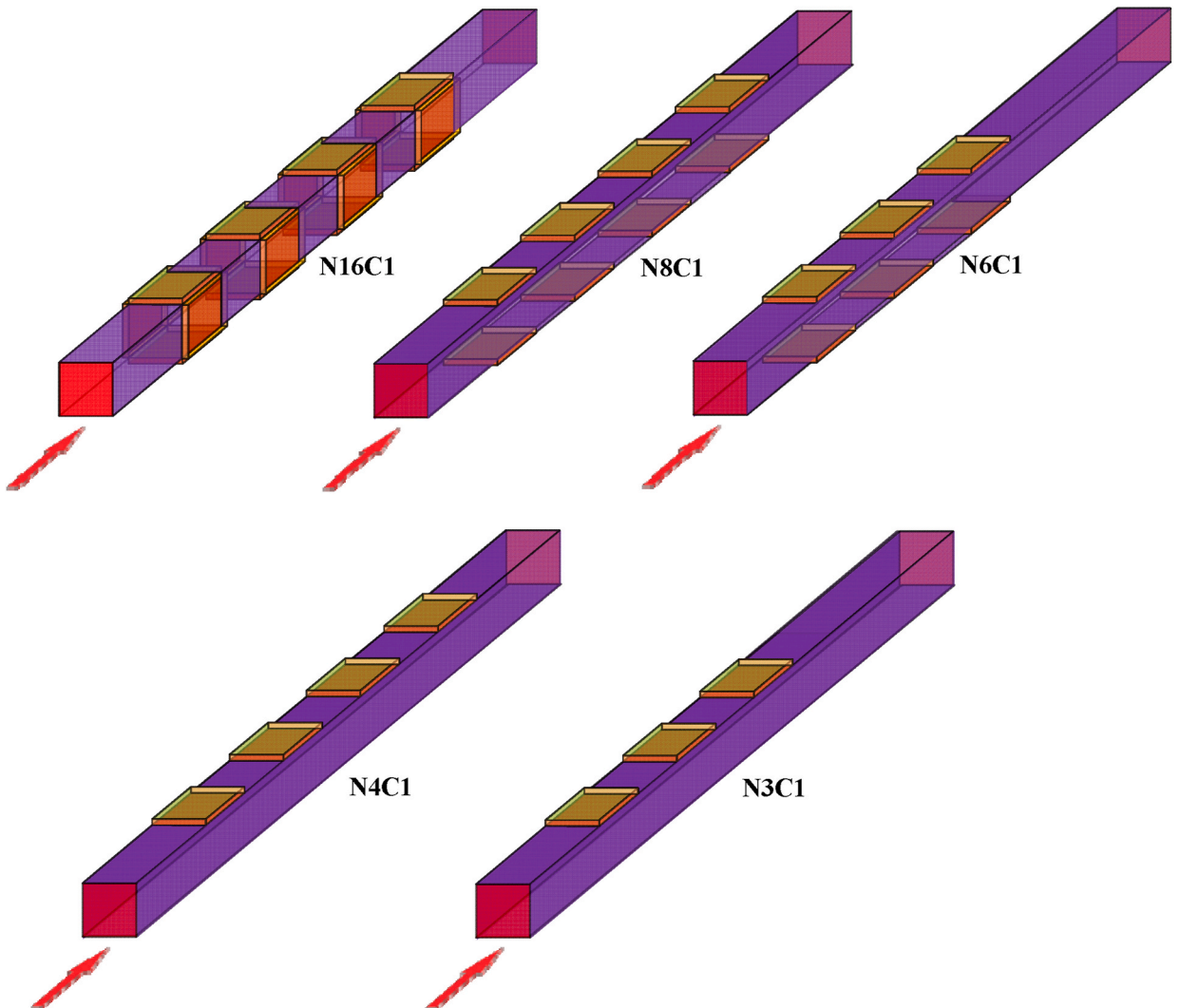


Fig. 9. TEG allocation with space for different number.

configuration of TEGs, where five different module numbers (16, 8, 6, 4, and 3) are chosen. The distance between modules in this configuration is equal to the width of a single TEG. In this arrangement, the remaining space between the TEGs is filled with insulating material, as depicted by the purple color in Fig. 9. This layout is referred to as C1 for convenience in subsequent discussions.

3.4.2. The effect of number module on output power and optimal TEG number

Fig. 10 illustrates the maximum net output power achieved with different numbers of modules when the inlet air temperature is 250 °C, both without a turbulator (left) and with a turbulator (right). In the absence of a turbulator, all new configurations, except for the one with 32 modules, show an improvement in power generation compared to the reference case. For instance, at an air flow rate of 24 kg/h, the output power increases by 22%, 12%, 29%, and 49% for the configurations with 16, 8, 6, and 4 modules, respectively. This indicates that these configurations can harvest more power from the hot air compared to the intimate configuration.

When considering the effect of the mass flow rate, the electric power output generally increases with an increase in the flow rate. Therefore, at a mass flow rate of 48 kg/h, the configuration with 8 modules yields the highest power output compared to other module numbers. However, the situation changes when a turbulator is introduced into the system. The results for configurations with a turbulator are somewhat different. The impact of the turbulator on power generation may alter the optimal module configuration for maximizing power output.

Although increasing the mass flow rate generally has advantages in terms of promoting power system performance and increasing power output, it is important to consider the balance between power generation and resistance power consumption in the channel. As the mass flow rate increases, the power output tends to increase until it reaches a maximum value. Beyond this point, further increases in the mass flow rate can lead to an increase in resistance power consumption, which can offset the additional power gained from the increased flow rate. Consequently, the total net power may start to decrease. This phenomenon occurs when the incremental power gained from the higher mass flow rate is not sufficient to compensate for the increased resistance power consumption. The net power output is then reduced due to the unfavorable balance between power generation and power consumption. Therefore, there exists an optimal mass flow rate that maximizes the net power output of the system. Operating the system at this optimal point ensures the most efficient utilization of the available heat source and minimizes power losses due to resistance power consumption.

3.4.3. Performance index for some experimental conditions

Based on the discussion, it is determined that the configuration with eight modules and the C1 layout demonstrates the best performance. To further investigate the characteristics of this configuration, additional experiments are conducted at an inlet air temperature (T) of 350 °C, as presented in Table 5. Table 5 reveals that the net output power and efficiency increase with an increase in the mass flow rate, regardless of the presence of a turbulator. However, the effect of the mass flow rate on the net power varies depending on whether a turbulator is present or not. The last two columns of Table 5 display the relative variation rates of the mass flow rate and net output power. It can be observed that the increase in net power becomes progressively slower, especially when a turbulator is present. For example, when the mass flow rate varies from 12 to 48 kg/h, the corresponding variation rates are 100%, 50%, and 33.3%. However, the variation rates of net power are 117.6%, 28.8%, and 5.3%. This indicates that the increase in net power becomes less significant as the mass flow rate increases, especially when a turbulator is involved. The variation tendency of the two variation rates suggests that the net output power may decrease once the mass flow rate reaches a certain value, similar to the observation at an inlet air temperature of 250 °C. Furthermore, the maximum net output power (16.93 W) and net efficiency (3.85%) are achieved at two different experimental conditions: T350Q48N8C1 and T350Q48N8C0. These values represent the peak performance observed in the experiments. For the C0 layout, the net output power reaches 14.1 W under the same experimental condition (T350Q48N8D1), indicating a 20% enhancement compared to the reference case. These results highlight the importance of carefully selecting the layout and operating conditions to optimize the net output power and efficiency of the thermoelectric system.

To analyze the reasons for the increase in output power with a non-compact arrangement, we conducted a simulation study of the temperature field inside the square duct. In the study, we assumed an inlet air temperature of 350 °C, an air flow rate of 48 kg/h, and a convective heat transfer coefficient between the hot air and the wall of 30 W/(m²·K). The number of thermoelectric elements was set to 3.

The simulation study, as depicted in Fig. 11, reveals distinct temperature characteristics between the compact and dispersed arrangements of thermoelectric elements. In the compact arrangement (left), the hot surface temperature remains relatively low and gradually decreases along the flow direction. However, in the dispersed arrangement (right), although the hot surface temperature is not high, the temperature of the walls in the gaps between the thermoelectric elements increases. Consequently, the average temperature of the subsequent thermoelectric elements' hot surfaces rises, leading to an increase in the output power. It is important to note that this simulation assumed a constant heat transfer coefficient. If we consider that the heat transfer coefficient is higher for the dispersed arrangement compared to the compact arrangement, the temperature distribution differences between the two arrangements will become even more pronounced.

4. Conclusion

The study conducted a series of experiments to investigate the performance of thermoelectric generator (TEG) modules and the impact of various factors on their performance. The following are the key findings of the study.

1. A new index called the power uniformity coefficient was introduced to assess the distribution of output power among TEGs. It was observed that as the mass flow rate increases and the number of modules decreases, the power uniformity coefficient increases. This indicates that the deviation of output power among TEGs gradually decreases under these conditions.

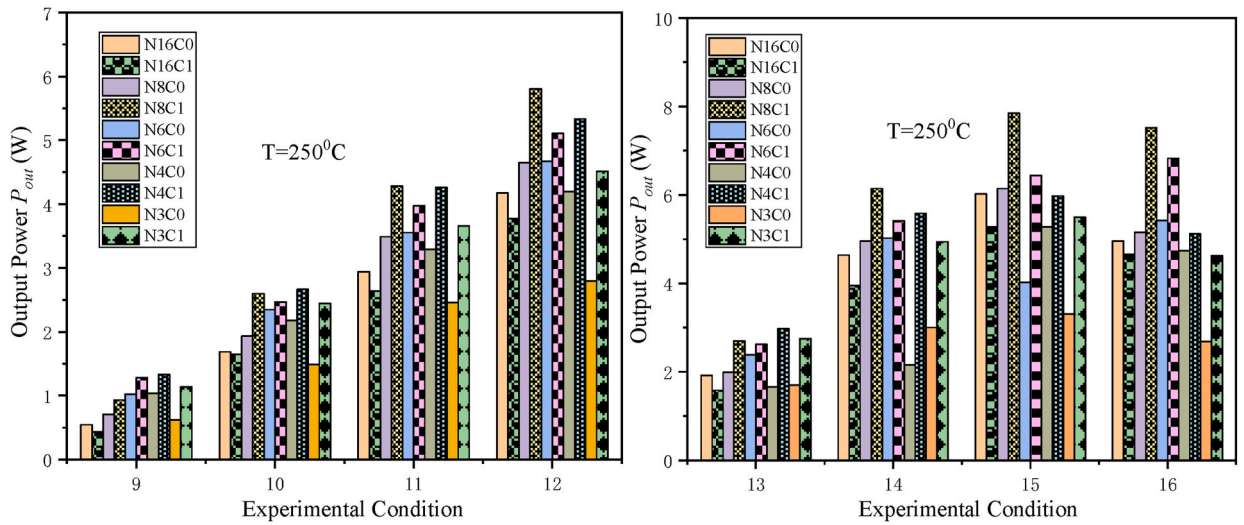


Fig. 10. Maximum net output power of different number modules for C0 and C1 layout.

Table 5
Summary of performance index ($N = 8, T = 350\text{ }^{\circ}\text{C}$).

| D | Q (kg/h) | TD ($^{\circ}\text{C}$) | P_{TEG} (W) | Δp (Pa) | P_w (W) | P_A (W) | P_{net} (W) | P_{per} (W) | $P_{\text{per,net}}$ (W) | η | η_{net} | $\Delta\eta_Q$ (%) | $\Delta\eta_{P_{\text{net}}}$ (%) |
|---|----------|---------------------------|----------------------|-----------------|-----------|-----------|----------------------|----------------------|--------------------------|--------|---------------------|--------------------|-----------------------------------|
| 0 | 12 | 32.77 | 2.30 | 0 | 0.21 | 0 | 2.09 | 0.29 | 0.26 | 1.97 | 1.79 | | |
| | 24 | 26.73 | 5.45 | 0 | 0.21 | 0 | 5.24 | 0.68 | 0.65 | 2.88 | 2.77 | 100 | 150.7 |
| | 36 | 23.66 | 8.54 | 0 | 0.21 | 0 | 8.33 | 1.07 | 1.04 | 3.49 | 3.40 | 50 | 58.9 |
| | 48 | 20.98 | 11.28 | 0 | 0.21 | 0 | 11.07 | 1.41 | 1.38 | 3.92 | 3.85 | 33.3 | 32.9 |
| 1 | 12 | 100.79 | 6.10 | 8.8 | 0.21 | 0.16 | 5.73 | 0.76 | 0.72 | 1.72 | 1.61 | | |
| | 24 | 82.02 | 13.44 | 37.8 | 0.21 | 0.76 | 12.47 | 1.68 | 1.56 | 2.36 | 2.19 | 100 | 117.6 |
| | 36 | 79.94 | 18.97 | 132.6 | 0.21 | 2.70 | 16.07 | 2.37 | 2.01 | 2.34 | 1.98 | 50 | 28.8 |
| | 48 | 59.22 | 22.75 | 270.6 | 0.21 | 5.61 | 16.93 | 2.84 | 2.12 | 2.97 | 2.21 | 33.3 | 5.3 |

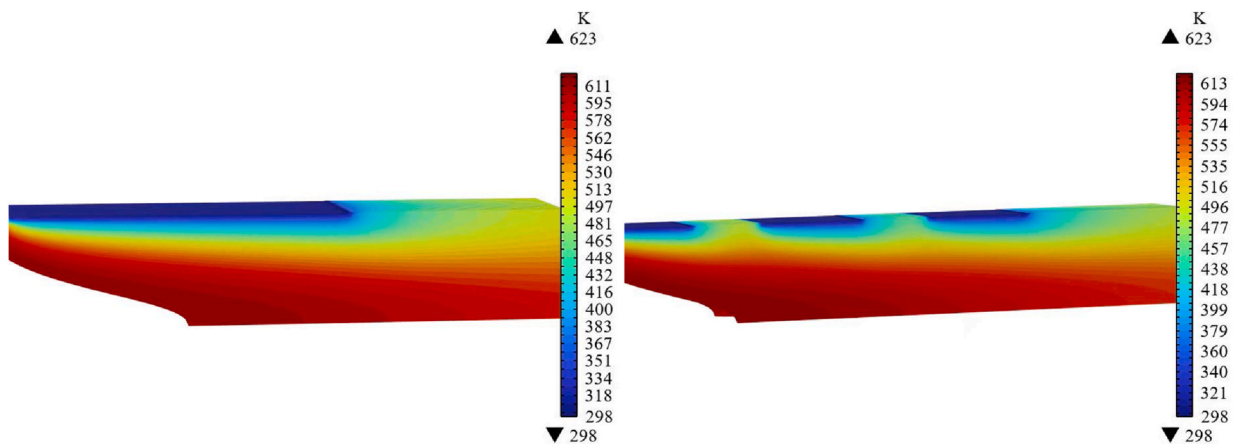


Fig. 11. The temperature field distribution for close and separate layout of TEG.

2. The optimum module number is found to be dependent on the working conditions, influenced by air temperature, mass flow rate, turbulator, etc., i.e. When the module layout is D0 (without a turbulator), six modules were found to be the best choice. However, when a turbulator is present, eight modules were determined to be the optimal configuration.
3. The layout of the TEG modules was found to have a significant effect on the performance of the thermoelectric system. The C1 layout, where the module number varies from 16 to 3, was observed to harvest more power from the hot air compared to corresponding C0 layout. This enhancement in power ranged from 10% to 50% and was observed regardless of the presence of a turbulator. Among the different module numbers, eight modules were consistently found to be the optimal configuration.

CRediT authorship contribution statement

Xiangrong Ma: Formal analysis, Validation, Writing – original draft. **Shenhua Hu:** Supervision. **Wuyuan Hu:** Data curation, Software.

Declaration of competing interest

The authors declare that they have no known competing financial interests or personal relationships that could have appeared to influence the work reported in this paper.

Data availability

Data will be made available on request.

Acknowledgments

This project has been supported by National Natural Science Foundation of China through Grant No. 51166013, the Innovation Fund General Programs I of Nanjing Institute of Technology (CKJB202106).

References

- [1] M. Fisac, F. Villasevil, A. López, High-efficiency photovoltaic technology including thermoelectric generation, *J. Power Sources* 252 (2014) 264–269.
- [2] J. Liu, S. Yadav, S. Kim, Performance of a thermoelectric generator system for waste heat recovery utilizing plate fin heat sink in bronze ingot casting industry, *Case Stud. Therm. Eng.* 38 (2022) 102340.
- [3] M. Aljaghtham, E. Celik, Design optimization of oil pan thermoelectric generator to recover waste heat from internal combustion engines, *Energy* 200 (2020) 117547.
- [4] N. Kanagaraj, Photovoltaic and thermoelectric generator combined hybrid energy system with an enhanced maximum power point tracking technique for higher energy conversion efficiency, *Sustainability* 13 (2021) 3144.
- [5] H. Hwang, K. Jang, Thermoelectric all-carbon heterostructures for a flexible thermoelectric generator, *Sustain. Energy Fuels* 5 (2021) 267–273.
- [6] K. Sornek, M. Filipowicz, M. Zoladek, et al., Comparative analysis of selected thermoelectric generators operating with wood-fired stove, *Energy* 166 (2019) 1303–1313.
- [7] P. Alegria, L. Catalan, M. Araiz, et al., Experimental development of a novel thermoelectric generator without moving parts to harness shallow hot dry rock fields, *Appl. Therm. Eng.* 200 (2022) 117619.
- [8] L. Zhu, T. Ding, M. Gao, et al., Shape conformal and thermal insulative organic solar absorber sponge for photothermal water evaporation and thermoelectric power generation, *Adv. Energy Mater.* 9 (2019) 1900250.
- [9] Q. Wan, Y. The, Y. Gao, et al., Analysis and design of a thermoelectric energy harvesting system with reconfigurable array of thermoelectric generators for IoT applications, *IEEE transactions on circuits and systems-i: regular papers* 64 (2017) 2346–2357.
- [10] I. Laird, D. Lu, High step-up DC/DC topology and MPPT algorithm for use with a thermoelectric generator, *IEEE Trans. Power Electron.* 28 (2013) 3147–3157.
- [11] H. Mamura, M. Üstüner, M. Bhuiyan, Future perspective and current situation of maximum power point tracking methods in thermoelectric generators, *Sustain. Energy Technol. Assessments* 50 (2022) 101824.
- [12] C.T. Hsu, G.Y. Huang, H.S. Chu, B. Yu, et al., Experiments and simulations on low-temperature waste heat harvesting system, *Appl. Energy* 88 (2011) 1291–1297.
- [13] Y. Li, S. Wang, Y. Zhao, et al., Experimental study on the influence of porous foam metal filled in the core flow region on the performance of thermoelectric generators, *Appl. Energy* 207 (2017) 634–642.
- [14] T. Wang, W. Luan, T. Liu T, et al., Performance enhancement of thermoelectric waste heat recovery system by using metal foam inserts, *Energy Convers. Manag.* 124 (2016) 13–19.
- [15] X. Lu, X. Yu, Z. Qu, et al., Experimental investigation on thermoelectric generator with non-uniform hot-side heat exchanger for waste heat recovery, *Energy Convers. Manag.* 150 (2017) 403–414.
- [16] X. Ma, S. Hu, W. Hu, et al., Experimental investigation of waste heat recovery of thermoelectric generators with temperature gradient, *Int. J. Heat Mass Tran.* 185 (2022) 122342.
- [17] K. Li, G. Garrison, M. Moore, et al., An expandable thermoelectric power generator and the experimental studies on power output, *Int. J. Heat Mass Tran.* 160 (2020) 1–8.
- [18] S. Samson, G. Li, X. Zhao, et al., Review of thermoelectric geometry and structure optimization for performance enhancement, *Appl. Energy* 268 (2020) 115075.
- [19] Y. Cui, B. Wang, J. Li, et al., Performance evaluation and lifetime prediction of a segmented photovoltaic-thermoelectric hybrid system, *Energy Convers. Manag.* 211 (2020) 112744.
- [20] S. Shittu, G. Li, X. Zhao, et al., Series of detail comparison and optimization of thermoelectric element geometry considering the PV effect, *Renew. Energy* 130 (2019) 930–942.
- [21] H. Lakeh, H. Kaatuzian, R. Hosseini, A parametrical study on photo-electro-thermal performance of an integrated thermoelectric-photovoltaic cell, *Renew. Energy* 138 (2019) 542–550.
- [22] Z. Xuan, M. Ge, C. Zhao, et al., Effect of nonuniform solar radiation on the performance of solar thermoelectric generators, *Energy* 290 (2024) 130249.
- [23] R. Lamba, S. Manikandan, S. Kaushik, et al., Thermodynamic modelling and performance optimization of trapezoidal thermoelectric cooler using genetic algorithm, *Therm. Sci. Eng. Prog.* 6 (2018) 236–250.
- [24] W. He, S. Wang, X. Zhang, et al., Optimization design method of thermoelectric generator based on exhaust gas parameters for recovery of engine waste heat, *Energy* 91 (2015) 1–9.

- [25] D. Jin, Z. Wei, J. Pou, et al., Geometry optimization of thermoelectric modules: simulation and experimental study, *Energy Convers. Manag.* 195 (2019) 236–243.
- [26] A. Negash, T. Kim, G. Cho, Effect of electrical array configuration of thermoelectric modules on waste heat recovery of thermoelectric generator, *Sensors Actuator, A Phys.* 260 (2017) 212–219.
- [27] J. Jang, Y. Tsai, Optimization of thermoelectric generator module spacing and spreader thickness used in a waste heat recovery system, *Appl. Therm. Eng.* 51 (2013) 677–689.
- [28] C. Favarel, J. Bédécarrats, T. Kousksou, et al., Numerical optimization of the occupancy rate of thermoelectric generators to produce the highest electrical power, *Energy* 68 (2014) 104–116.
- [29] C. Alvaro, A. Miguel, C. Leyre, et al., Thermoelectric heat recovery in a real industry: from laboratory optimization to reality, *Appl. Therm. Eng.* 184 (2021) 116275.
- [30] A. Rattner, T. Meehan, Simple analytic model for optimally sizing thermoelectric generator module arrays for waste heat recovery, *Appl. Therm. Eng.* 146 (2019) 795–804.
- [31] A. Miguel, C. Alvaro, C. Leyre, et al., Prospects of waste-heat recovery from a real industry using thermoelectric generators: economic and power output analysis, *Energy Convers. Manag.* 205 (2020) 112376.
- [32] Y. Zhao, W. Li, X. Zhao, et al., Energy and exergy analysis of a thermoelectric generator system for automotive exhaust waste heat recovery, *Appl. Therm. Eng.* 239 (2024) 122180.
- [33] A. Patricia, C. Leyre, A. Miguel, et al., Thermoelectric generator for high temperature geothermal anomalies: experimental development and field operation, *Geothermics* 110 (2023) 102677.
- [34] W. He, Z. Cai, R. Guo, et al., Effect of exhaust thermal parameters on optimal circuit layouts and optimal thermoelectric generator structure used in internal combustion engine, *Energy Convers. Manag.* X 19 (2023) 100388.
- [35] M. Ge, Z. Li, Y. Zhao, et al., Experimental study of thermoelectric generator with different numbers of modules for waste heat recovery, *Appl. Energy* 322 (2022) 119523.
- [36] Z. Shen, L. Tian, X. Liu, Automotive exhaust thermoelectric generators: current status, challenges and future prospects, *Energy Convers. Manag.* 195 (2019) 1138–1173.
- [37] S. Kline, F. McClintock, Describing uncertainties in single-sample experiment, *Mech. Eng.* 75 (1953) 3–8.
- [38] C. Weng, M. Huang, A simulation study of automotive waste heat recovery using a thermoelectric power generator, *Int. J. Therm. Sci.* 71 (2013) 302–309.